ELSEVIER

Journal of Neuroscience Methods 124 (2003) 45–59

JOURNAL OF NEUROSCIENCE METHODS

www.elsevier.com/locate/jneumeth

Differential tissue shrinkage and compression in the *z*-axis: implications for optical disector counting in vibratome-, plastic- and cryosections

Dean Gardella [a], William J. Hatton [b], Howard B. Rind [a], Glenn D. Rosen [c], Christopher S. von Bartheld [a,*]

[a] *Department of Physiology and Cell Biology, Mailstop 352, University of Nevada School of Medicine, Reno, NV 89557, USA*
[b] *Department of Pharmacology, University of Nevada School of Medicine, Reno, NV 89557, USA*
[c] *Dyslexia Research Laboratory and Charles A. Dana Research Institute, and Department of Neurology, Division of Behavioral Neurology, Beth Israel Deaconess Medical Center, Harvard Medical School, Boston, MA, USA*

Received 2 July 2002; received in revised form 9 December 2002; accepted 11 December 2002

Abstract

The optical disector is among the most efficient cell counting methods, but its accuracy depends on an undistorted particle distribution in the *z*-axis of tissue sections. Because the optical disector samples particle densities exclusively in the center of sections, it is essential for unbiased estimates of particle numbers that differential shrinkage or compression (and resulting differences in particle densities along the *z*-axis) are known and corrected. Here we examined, quantified, and compared differential shrinkage and compression of vibratome-, celloidin- and cryosections. Vibratome sections showed a significant *z*-axis distortion, while celloidin- and cryosections were minimally distorted. Results were directly compared with previous data obtained from paraffin and methacrylate sections. We conclude that *z*-axis distortion varies significantly between embedding and sectioning methods, and that vibratome-, methacrylate- and paraffin sections can result in grossly biased estimates. We describe a simple method for assessing differential *z*-axis shrinkage or compression, as well as simple strategies to minimize the bias of the optical disector. Minimal bias can be achieved by either adjusting the placement and extent of counting boxes and guard spaces for sampling, or by applying a correction factor in cases when guard spaces are deemed essential for particle recognition.

Keywords: Optical disector; Stereology; Vibratome section; Celloidin; Compression; Sampling; Particle counting; Bias

1. Introduction

Quantitative morphology is important in developmental, clinical and aging biology. In order to evaluate the progression of degenerative diseases, or to evaluate the effects of mechanical or pharmacological manipulations in animals, it is important to quantify the extent of cell survival. In order to quantify changes in particle number in tissues, such tissues have to be sectioned. The most straightforward and direct method for cell counting is to fix the tissue of interest, prepare sections through the tissue, stain the sections, and to count the cells under the microscope.

Previous techniques used 'profile counting' (two-dimensional (2D) counting, counting of each profile of each particle in equally spaced, thin sections, Clarke and Oppenheim, 1995), often followed by application of correction factors for overcount because larger particles are sectioned into more than one profile, resulting in an overcount due to multiple profiles per particle (Abercrombie, 1946; Konigsmark, 1970; Clarke, 1993). The correction procedure was criticized because of assumptions that have to be made about the size, shape and orientation of particles, resulting in significant biases (Gundersen et al., 1988a,b; Coggeshall and Lekan, 1996; Hedreen, 1998b). About 15 years ago, new counting techniques were introduced which count samples in 3D

* Corresponding author. Tel.: +1-775-784-6022/4635; fax: +1-775-784-6903.
E-mail address: chrisvb@physio.unr.edu (C.S. von Bartheld).

0165-0270/03/$ - see front matter
doi:10.1016/S0165-0270(02)00363-1

space and then apply such representative samples to the total reference space (Gundersen et al., 1988a,b; Williams and Rakic, 1988; Howard and Reed, 1998). This approach uniquely identifies each particle and abolishes the counting of profiles. It is most efficient to use 'optical sections' that define a counting box within thick tissue sections (hence the name 'optical disector') rather than to align two images from adjacent (or subsequent) thin sections (the 'physical disector'). To avoid cutting artifacts at section surfaces and to identify particles unambiguously, it was recommended to sample particle densities only in the core of the tissue sections, but to avoid the margins ('guard spaces') (Gundersen et al., 1988a,b; Howard and Reed, 1998; Andersen and Gundersen, 1999).

Until recently, the new 3D counting techniques were thought to be unbiased (Gundersen et al., 1988a,b; Cruz-Orive, 1994; Mayhew and Gundersen, 1996; Howard and Reed, 1998). Our own and others' work has shown that one important assumption has to be made with the optical disector when one uses guard spaces: one has to assume that there is no differential shrinkage or compression of tissue sections in the z-axis. If there is differential shrinkage or compression of tissue sections (Fig. 1), one can not sample exclusively in the core of tissue sections. In other words, one may not exclude the margins of tissue sections ('guard spaces'), because the core of the sections does not contain a representative density of particles (Hatton and von Bartheld, 1999; von Bartheld, 1999, 2001; Dorph-Petersen et al., 2001). Differential shrinkage or compression of sections can significantly bias the optical disector method, by as much as 25% (Hatton and von Bartheld, 1999).

To date, only three of the five commonly-used types of tissue sections have been examined for the extent of differential compression or shrinkage in the z-axis: paraffin-, cryosections, and methacrylate resin sections (Hatton and von Bartheld, 1999), but vibratome sections have not been thoroughly analyzed (Andersen and Gundersen, 1999), and celloidin sections have not been tested at all, despite the fact that celloidin sections are increasingly used for optical disector counting (Avendano and Dykes, 1996; Herman et al., 1997; Selemon et al., 1998; Heinsen et al., 2000; Rosen and Williams, 2001). Here we provide a detailed analysis of both vibratome sections and celloidin plastic sections, and compare them directly with cryosections, all for the same type of large motor CNS neurons, the oculomotor nuclei. In addition, we provide a simple protocol (Section 2.3, that can be used by any investigator with a set-up for optical disector counting) for quantification of the distortion of tissue sections in the z-axis. We report on the extent to which all major tissue section types can be affected by differential distortion, and how

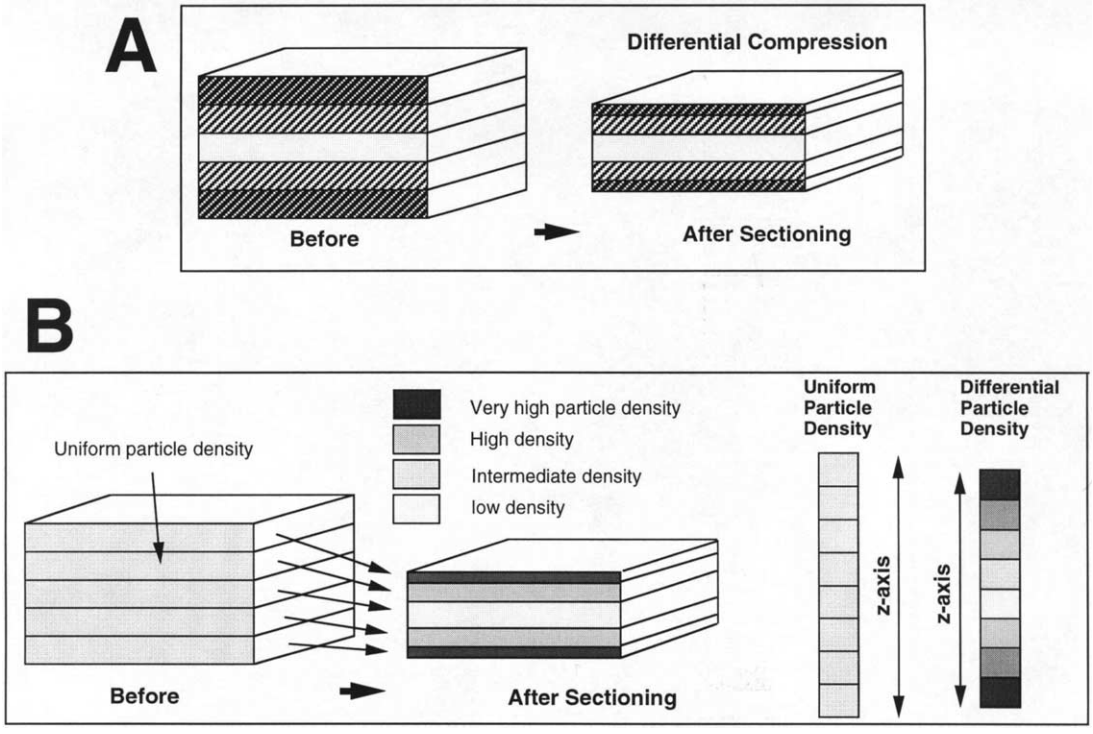

Fig. 1. Deformation of tissue sections in the direction of the z-axis due to compression during sectioning. (A) The tissue block on the left side shows five zones within the z-axis. Prior to sectioning, they are of equal size. After sectioning, differential compression renders the zones at the margins more compressed (A), while the center zone is not affected. (B) Uniform particle density in the original tissue block is thus transformed into zones containing differential particle densities as illustrated. If one were to take samples of particle density in the z-axis before and after sectioning, one would find uniform particle density before, but differential particle density after sectioning (right hand of panel B).

this problem can be easily and successfully dealt with (Section 4.5). While our study is particularly relevant for optical disector particle counting, it addresses in a broader scope problems that affect all methods that rely on sampling outside of guard zones as being representative for the entire section. Preliminary data of this work have been reported in abstract form (Gardella et al., 2002).

2. Methods

2.1. Animals

Fertilized White Leghorn chicken eggs were obtained from local suppliers and were incubated in humidified incubators at 37.0–37.5 °C. Hatchling chicks were anesthetized with sodium-pentobarbital (Nembutal, 50 mg/kg body weight) prior to perfusion or decapitation. Adult mice were obtained from the Jackson Laboratories (Bar Harbor, ME) and anesthetized with Avertin (0.5–0.8 ml, i.p.). Adult guinea pigs were obtained from Simonsen Laboratories, Inc. (Gilroy, CA) and anesthetized with isoflurane followed by exsanguination (courtesy of Dr Nick Spencer, University of Nevada, Reno). The numbers of animals used, sections analyzed, samples taken, and neurons measured are summarized in Table 1. Experimental procedures were conducted in compliance with the Policy on the Use of Animals in Neuroscience Research and were approved by the local animal care committees.

Table 1
Numbers of animals, sections, samples ('counting boxes') and cells analyzed for z-axis distortion with different embedding or sectioning methods as shown in Figs. 2–4

Method	Animals (#)	Sections (#)	Samples (#)	Cells (#)
Vibratome	3	10	49	616
Investigator 1		4	17	264
Investigator 2		6	32	352
Celloidin	2	12	81	909
Investigator 1		3	20	234
Investigator 2		4	31	270
Investigator 3		5	30	405
Cryostat	5	9	62	630
Investigator 1		3	29	162
Investigator 2		6	33	468
Paraffin[a]	5	11	82	827
Investigator 1		6	50	543
Investigator 2		5	32	284
Glycolmethacrylate[a]	5	14	56	494
Investigator 1		5	22	157
Investigator 2		9	34	337
Aqueous mount	2	5	23	315
Investigator 1		3	18	214
Investigator 2		2	5	101
Thick cryosections	3	6	25	321

Additional paraffin and glycolmethacrylate data (not listed here) were obtained for thick (40–50 μm) sections.
[a] Data from Hatton and von Bartheld (1999).

2.2. Tissue processing

2.2.1. Vibratome sections

Animals were anesthetized and perfused with cold 4% paraformaldehyde (PFA) in phosphate-buffered saline (PBS, pH 7.5). Brains were postfixed for 2–4 h, dissected, the forebrain was trimmed, and the brainstem was glued to a metal chuck with super glue plus™ (Kwik Fix®). The chuck was mounted on a vibratome (series 1000), the chamber filled with PBS, and sections were cut at 60–120 μm with Gillette (super stainless) or Schick razor blades. The settings on the vibratome were adjusted to a speed of 4.5, an amplitude of 3.75, and a nominal section thickness of 80 μm, so that the final, dehydrated and coverslipped sections were 25–35 μm thick. A nominal section thickness of 80 μm resulted in a final thickness of 31.78 μm (mean, SEM = 0.45, $n = 32$). A nominal section thickness of 100 μm resulted in a final thickness of 46.50 μm (mean, SEM = 0.92, $n = 6$). Sections were collected on silane- or gelatine-coated glass slides (Fisherbrand® Microscope Slides, 25 × 75 × 1 mm^3, Fisher Scientific, Pittsburgh, PA), dried, and stained with 0.03% thionin. Sections through the midbrain containing oculomotor nuclei were dehydrated in a series of graded ethanols, cleared in xylene, and coverslipped with #1–1/2 Corning® cover glasses (Corning Inc., Corning, NY), using D.P.X. mounting medium (Electron Microscopy Sciences, EMS, Fort Washington, PA) with a refractive index of 1.52. Particular attention was given to the upper and lower surfaces of vibratome sections to determine if the margins of tissue sections were depleted of neuronal nuclei as suggested in a previous study (Andersen and Gundersen, 1999).

2.2.2. Celloidin sections

Brains were embedded in celloidin as described in detail elsewhere (Rosen and Williams, in press). In brief, mice were anesthetized with Avertin (0.5–0.8 ml, i.p.) and were perfused transcardially with 0.9% PBS followed by approximately 15 ml of 1.25% glutaraldehyde and 1.0% PFA in 0.1 M phosphate buffer. An additional 10–20 ml of double-strength fixative (2.5% glutaraldehyde and 2.0% PFA in the same buffer) was subsequently injected for 1–2 min at an increased rate and pressure. The head was removed and placed in the final fixative until the brain was dissected. The brains were subsequently fixed in 10% formalin for 2 weeks prior to embedding. Following washes in distilled water and dehydration with graded ethanols, they were immersed

in a 1:1 solution of 100% ethanol and ether before being embedded for 1 week in a 3% solution of celloidin in a 1:1 solution of 100% ethanol and ethyl ether, followed by 12% celloidin for 3 days. After hardening, the blocked brains were sectioned on a sliding microtome at 30 μm. A nominal section thickness of 30 μm resulted in a final thickness of 27.47 μm (mean, SEM = 0.16, n = 19). Sections were stored in 80% ethanol, and a 1-in-10 series was stained free-floating with 0.5% cresyl-violet. After clearing in terpineol and xylene, sections were mounted on Fisher-Brand (Fisher Scientific, Chicago, IL) slides (50×75 mm^2) and coverslipped with Permount (Fisher Scientific, refractive index (dry) = 1.529).

2.2.3. Cryosections

Animals were anesthetized and perfused with cold 4% PFA in PBS, pH 7.5. Brains were postfixed for 4 h, dissected, washed in PBS (30 min), and cryoprotected in 30% sucrose in PBS overnight at 4 °C. The forebrain was trimmed, and the brainstem was embedded in O.C.T. compound (Tissue Tek®), and frozen onto a metal chuck using crushed dry ice. Cryosections were cut at 40–100 μm in a Leica cryostat (CM 3050, rotary microtome) using disposable low profile metal blades (Accu-Edge®). The nominal section thickness on the cryostat was adjusted to 60 μm so that the final, dehydrated and coverslipped sections were 30–40 μm thick. A nominal section thickness of 60 μm resulted in a final thickness of 37.08 μm (mean, SEM = 1.32, n = 12). Sections were collected on silane- or gelatine-coated glass slides, dried, and stained with 0.03% thionin. Sections were dehydrated in a series of graded ethanols, cleared in xylene, and coverslipped with D.P.X. mounting medium.

2.2.4. Paraffin sections

The heads of hatchling chicks and one adult guinea pig midbrain were fixed in Methacarn (methanol, chloroform and acetic acid at volume ratios of 6:3:1). One hatchling chick was perfused transcardially with 0.9% PBS followed by approximately 15 ml of 1.25% glutaraldehyde and 1.0% PFA in 0.1 M phosphate buffer and an additional 10–20 ml of double-strength fixative (2.5% glutaraldehyde and 2.0% PFA in the same buffer). The brains were dissected, dehydrated in methanol, cleared in xylene, and embedded in paraffin (Paraplast Plus, Oxford Labware) at 58 °C, solidified at 4 °C, and sectioned at 25–35 μm at room temperature. For Methacarn-fixed tissue, a nominal section thickness of 25 μm resulted in a final thickness of 23.38 μm (mean, SEM = 0.81, n = 13). For glutaraldehyde-fixed tissue, a nominal section thickness of 35 μm resulted in a final thickness of 27.20 μm (mean, SEM = 0.89, n = 10). Sections through oculomotor or isthmic nuclei (nucleus isthmi, pars magnocellularis) were collected on gelatine- or silane-coated slides, deparaffinized in xylene, hydrated in a graded ethanol series, and stained with thionin. Chick brain sections were coverslipped with aqueous mounting media (GEL/MOUNT™, Biomeda Corp., refractive index = 1.36, or Aqua-Mount®, Lerner Laboratories), or dehydrated in a graded ethanol series, cleared in xylene and coverslipped with D.P.X. mounting medium (some chick brain sections and all guinea pig brain sections).

2.3. Section analyses

Sections were viewed with a 40× objective on a Nikon Optiphot microscope to identify motor nuclei. The scope was equipped with a drawing tube (Nikon 1.25) and a microcator (MFC-1 focus controller and DRV-1 OPTI drive with a digital read-out, Applied Scientific Instrumentation, Inc., Eugene, OR). A 2D point intersect overlay (a grid with 100 points situated in the eye piece) was used with a 100× immersion oil objective (NA = 1.25) to analyze the neuronal nuclei. We used Resolve microscope immersion oil (high viscosity, Stephens Scientific, Kinnelon, NJ) with a refractive index = 1.5150 at 23 °C. For each frame, the thickness of the section was measured by focusing on the upper and lower section surfaces; the abundant small glial cells proved particularly useful for this task. Measurements of the section thickness and depth of focus in stereology always involve some subjective judgement, as discussed in detail elsewhere (Uylings et al., 1986; Guillery, 2002). Determination of the section thickness may be facilitated and verified objectively by employing an auto-focus device and read-out (e.g. ASI's video auto-focus with a MS-2000 XYZ stage or MFC-2000 Z-drive, Applied Scientific Instrumentation).

The position of nuclei in the z-axis of tissue sections was determined for motoneurons (oculomotor, trochlear and abducens neurons) and isthmic neurons in cryo-, vibratome and celloidin sections. Using an unbiased counting rule, neurons were scored only when the center of the neuronal nucleus was within the counting frame and within the tissue section, as determined by focusing through the tissue section using a microcator with a resolution of 0.1 μm. To measure the position of particles in the z-axis, we used counting boxes defined by a grid in the eye piece with an xy area of between 640 and 6400 μm^2, and the size of the counting box was adjusted to the particle density so that between 5 and 25 particles were scored per counting box. The microcator was directly mounted on the focusing knob (Applied Scientific Instrumentation) and calibrated by measuring a standard 1 mm thick glass slide with 20× air objectives, taking Snell's law into account. The thickness of the glass slide was verified with a micrometer scale to be 1.00 ± 0.02 mm. Centers of nuclei were measured, rather than 'tops' of nuclei, because measuring only tops would distort the

results, as one would count particles at the upper surface only when their tops are within the tissue, but one would count every and all the tops (even the smallest tops) at the bottom surface. This would result in an asymmetric distribution profile, because the distance between the top and the bottom of the nuclei is about 6–8 μm, which would be reflected in such measurements. Second, it would be very difficult to identify very small tops at the bottom surface, because they do not have the rest of the nucleus associated with them to facilitate their identification.

Counting centers of nuclei is more reliable than counting tops at the section surfaces, because one has at least half of the nucleus associated with the center—if one has less than half the center of the nucleus associated, then (by definition!) the nucleus should NOT be counted. The center of the nucleus was defined by focusing on the clear nuclear edge and the most clearly defined nuclear chromatin (Nurcombe et al., 1991; Howard and Reed, 1998). This approach was adopted from Nurcombe, Gundersen, Howard and colleagues who state that 'Nuclei were counted'... when 'the nuclear edge and associated chromatin was most clearly defined' (Nurcombe et al., 1991), that 'one focusses through the nucleus and... simply counts these neurons when their sharpest nuclear profile falls within the disector counting frame' (Gundersen et al., 1988a), or when 'the nuclear membrane of each cell nucleus comes into sharpest focus within the field of view...' (Howard and Reed, 1998, p. 87).

Measurements were taken for each neuronal nucleus within the counting frame (usually between 5 and 25 particles), and the z-axis position of the center of the nucleus was recorded as seen in the digital read-out of the microcator (Hatton and von Bartheld, 1999). Split nuclei were counted only when the center of the nucleus was clearly within the tissue section. This was established by comparing the radius (1/2 of the diameter measured in the x/y axes) with the z-axis fragment of the nucleus. The radius can be used, because the xy- and z-values for nuclei do not differ significantly for paraffin and cryosections (Hatton and von Bartheld, 1999) and vibratome sections (data not shown), despite the z-axis distortion, and are relatively minor for methacrylate resin sections (Hatton and von Bartheld, 1999) and celloidin sections (data not shown). For each condition, 4–6 groups of 75–150 neurons each were scored and grouped in 10 histograms from the percentiles 0–100 through the tissue section from the upper surface (0%) to the lower surface (100%). Statistical analyses indicate that a minimum of 250–350 particles need to be scored to identify distortion in the z-axis (Section 2.5 below).

In addition to measurements of 'centers of nuclei', the distribution of centers of nucleoli was determined in celloidin and paraffin material. This was not routinely possible in vibratome and cryosections because the nucleolus was identifiable only in a fraction of all neurons. Nucleoli are less likely than nuclei to be split by the knife, because they are smaller and 'harder' than nuclei, and nucleoli tend to be 'pushed and rolled rather than cleanly cut by the knife' (Coggeshall and Chung, 1984). When they can be recognized, nucleoli provide better resolution than nuclei (Clarke and Oppenheim, 1995), and it can be difficult to recognize small fragments of 'tops' of nuclei (Hedreen, 1998a). The density distribution analyses were used to calculate the predicted bias of the optical disector method, a bias that results from sampling in non-representative zones within the core of sections (Section 4.5).

2.4. Control sections

To determine the influence of uneven staining (in case of staining of sections collected and dried onto glass slides), thicker cryosections (45–55 μm) were analyzed that had been stained with thionin, but where the stain had not penetrated entirely through the section thickness. In short, the hatchling chicks were perfused transcardially with 4% PFA, the brains frozen in O.C.T. compound, and sectioned in the cryostat at a nominal thickness of 80–100 μm. The final section thickness was 49.44 μm (mean, SEM = 0.74, $n = 25$). Although particles at the bottom surface of the section were stained much lighter, it was possible to measure the section thickness by focusing on lightly-stained particles. Sections through the oculomotor and parabigeminal nuclei of one adult guinea pig were analyzed in the same way as described above; each visible center of a nucleus or nucleolus was measured.

2.5. Statistical analyses of z-axis distortion

Statistical analyses were performed using SIGMASTAT software (SPSS Science, Chicago, IL) and STATVIEW (SAS Institute, Cary, NC). One-way analysis of variance (ANOVA) was used to assess the distribution of particles in the z-axis from vibratome-, celloidin-, and cryosections (Fig. 2A–C). For each set of data analyzed, significant differences between the groups were taken as evidence that particle density was non-uniform through the z-axis. χ^2-tests against the expected distribution were used to confirm the ANOVA, and post-hoc contribution of each bin was determined. Particles from each of the sections were grouped in one of 10 bins based on their distance from the surface of the section. Thus, a particle contained within the first 2 μm of a 30 μm section would be placed in the first bin (0–10%), while a particle found 16 μm from the surface would be placed in the 50–60% bin. Ten percent represents the fraction of particles that would be expected in each of the ten bins through the z-axis if such particles were uniformly distributed. Ten percent bin sizes as well as 20% bin sizes were tested for

χ^2. For the numbers of animals, sections, samples and cells analyzed, see Table 1.

To determine how many particles need to be measured to obtain statistically meaningful results, we empirically determined how many particles were required to see statistical significance in the set of data with 616 particles in the vibratome sections. ANOVA was used to identify if the mean values (% of neuronal nuclei) differed significantly between the 10 bins. The mean% of particles present in each bin was derived by taking the 616 total nuclei counted in this analysis and segregating them into clusters of 7 groups (each representing 88 nuclei). The 616 nuclei analyzed were derived from a total of 49 counting boxes, thus resulting in 7 groups, each group consisting of 7 counting boxes. The final mean value for each bin was calculated by determining the mean value of these 7 groups. ANOVA was initially run on all 616 nuclei (all 7 groups). To determine how many groups and nuclei were required, in this data set, to show significant differences between bins, we then randomly and systematically reduced the data, 1 group at a time (e.g. 7 counting boxes with 88 nuclei at a time) and ran ANOVA each time. For example, from the 7 groups (616 nuclei), 1 group was randomly chosen, eliminated, and ANOVA run on the remaining data (6 groups with 42 counting boxes and 528 nuclei). To further reduce the data, an additional group was randomly chosen and eliminated, and ANOVA run on the remaining data (5 groups with 35 counting boxes and 440 nuclei). We continued this process until the resulting ANOVA produced a value of $P > 0.05$.

To determine if the final dehydration step in processing paraffin sections was responsible for the observed z-axis distortion, the patterns of particle densities through the z-axis were compared between dehydrated and aqueous mounted paraffin sections using the Spearman rank order correlation test.

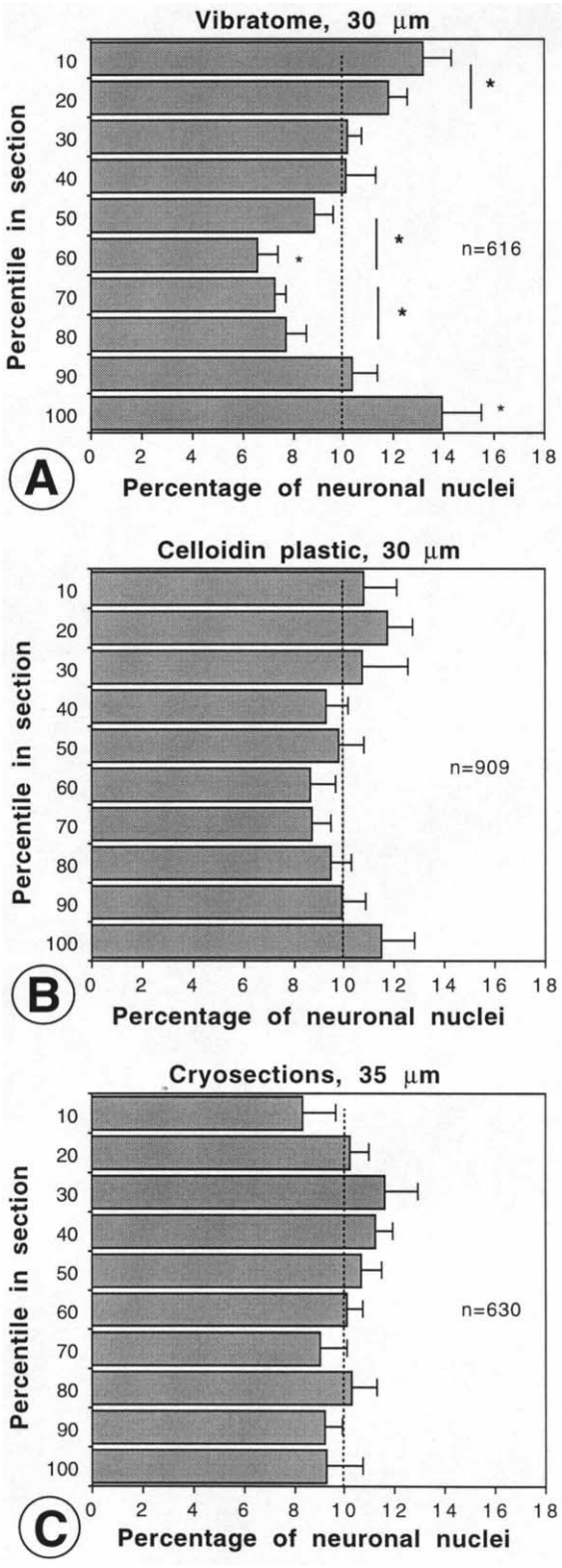

Fig. 2

Fig. 2. (A–C) Distribution of particles in the z-axis of vibratome sections (A), celloidin sections (B) and cryosections (C). Note that vibratome sections show a bimodal but symmetric pattern with significantly increased particle densities at both margins, and significantly lower densities in the core of the section. Statistical significance compared with the expected 10% value (dotted line) was determined by χ^2-test with 10 percentile bins (small *) as well as 20 percentile bins (large *). The pattern for celloidin sections is nearly flat, with a very slight, but statistically insignificant, decrease towards the core of the section. The pattern for cryosections is almost flat, with a slightly lower density at both margins (statistically insignificant with the χ^2-test). The total number of particles measured (n) is indicated. The top 0–10% bin of the tissue section (against the cover slip) is the '10' percentile, the bottom bin (90–100%) of the section (against the glass slide) is the '100' percentile. All data shown were grouped in 10s of percentiles (0–10% = '10'; 10–20% = '20';. . ..90–100% = '100'). The vertical dashed line indicates how the particles would present if all particles were equally distributed throughout the z-axis (10% of all particles in 10% of all bins). Error bars = SEM. See Section 2 (Section 2.5) for details on the statistical analyses.

3. Results

3.1. z-axis distortion in vibratome sections

Vibratome sections are often used in immunocytochemical studies, because antibodies penetrate such sections more readily (e.g. Stuart and Oorschot, 1995; Dorph-Petersen et al., 2001). A previous study has emphasized the need for guard spaces when the optical disector is used on vibratome sections, because of a depletion of particles in the margins of vibratome sections (Andersen and Gundersen, 1999). Our vibratome sections of 25–35 μm thickness showed no evidence of reduced densities of particles in the margins of sections (Fig. 2A), but on the contrary a rather large increase in the density of particles (motor neurons) at the margins, indicating a substantial distortion within the z-axis of vibratome sections. ANOVA revealed that this distortion in the z-axis was significant, as the bins shown in Fig. 2A differed significantly from each other ($F_{8,54} = 6.24$, $P < 0.001$). χ^2 analyses showed significant differences from the expected distribution ($\chi^2 = 17.85$, d.f. $= 9$, $P < 0.05$, Fig. 2A). The 50–60% and the 90–100% bins contributed significantly to the χ^2. When the bins were grouped into five 20% bins instead of ten 10% bins, the 0–20%, 40–60%, and 60–80% bins contributed significantly to the Chi-square ($\chi^2 = 14.77$, d.f. $= 4$, Fig. 2A). We conclude that there was no loss of particles at the margins, but rather a higher density in the margins, presumably reflecting compression during sectioning. When the bin size was reduced from 10 to 5%, the same effect was noted, i.e. compression seems to affect the entire 15% percent of the upper bins, and the entire 10% of the lower bins (facing the glass slide, data not shown). The distortion was symmetrical, with both surface zones containing 30–40% increased densities of cells, and a statistically significant drop-off towards the center of the tissue section to about 60% of average. This pattern of differential distribution of particles in the z-axis was consistently observed and highly reproducible (note the size of the error bars in Fig. 2A). Reducing the total number of particles analyzed (from 616) in steps of 88 nuclei (as detailed in Section 2) showed that between 250 and 350 particles needed to be measured and counted for ANOVA to reproducibly identify statistically significant distortion in the z-axis of these vibratome sections.

3.2. z-axis distortion in celloidin sections

As mentioned above, celloidin embedding is increasingly used in quantitative morphology, including optical disector studies (e.g. Herman et al., 1997). Our celloidin sections of 30 μm thickness showed an even distribution of neuronal nuclei in the z-axis, as the bins were not significantly different from one another ($F_{9,90} < 1$, ns). When nucleoli instead of centers of nuclei were measured, the results were virtually identical (data not shown), and therefore the two groups were combined for graphing (Fig. 2B). There was a slight (but statistically insignificant) trend towards higher densities at both surface zones, and a very minor zone of lower densities in the center of the tissue section that never dropped below 8.5% for any bin, compared with the theoretical average of 10% (Fig. 2B). The χ^2-test showed no significant differences compared with the expected 10% value ($\chi^2 = 4.49$, d.f. $= 9$, ns). The pattern of distribution of particles in the z-axis was symmetric, as shown in Fig. 2B. As can be seen from the size of the error bars, this pattern was consistent among our sections.

3.3. z-axis distortion in cryosections

Cryosections have previously been examined for differential z-axis distortion (Hatton and von Bartheld, 1999), but since the results were somewhat unexpected and surprising (lack of any major distortion, despite the significant shrinkage in the z-axis due to drying, Hatton and von Bartheld, 1999; Schmitz et al., 2001; Dorph-Petersen et al., 2001), we here tested the distortion with a new series of cryosections for direct comparison with both the vibratome and celloidin sections. Consistent with our previous results (Hatton and von Bartheld, 1999), the current analysis failed to demonstrate significant differences in particle density through the z-axis ($F_{9,70} = 1.02$, ns). The χ^2-test showed no significant differences compared with the expected 10% value ($\chi^2 = 2.88$, d.f. $= 9$, ns). The cryosections of 30–40 μm thickness showed a symmetric pattern, with a trend towards a slight increase in densities of oculomotor neuron nuclei in the center of the section, and a drop-off towards both the upper surface and the lower surface (Fig. 2C). As seen from the size of the error bars, this pattern was consistent. Such a pattern could be caused by differential shrinkage, but the same pattern would also be seen if some particles were lost at both the upper and lower surfaces, due to cutting artifacts and uneven surfaces. We cannot distinguish between these two possibilities, or even a combination of the two effects. Even if the increased densities at the center of the tissue sections were real, they were less than about 5%, and thus would cause a bias smaller than about 5% in particle estimates obtained with the optical disector, as concluded in our previous study (Hatton and von Bartheld, 1999).

3.4. Effects of uneven stain penetration and other parameters on apparent z-axis distribution of particles

Since reported uneven particle distribution in the z-axis of tissue sections has been associated with possible

'poor stain penetration' (Dorph-Petersen et al., 2001), we examined the pattern of apparent particle distributions in thick (45–55 μm) cryosections collected on glass slides in which the stain failed to penetrate entirely through the tissue section. As can be seen in Fig. 3F, the pattern shows a strong asymmetry, with higher densities at the surface and throughout the upper 70–80% of the tissue section, and a sharp drop-off (as low as 50%) towards the lower surface (adjacent to the glass surface) of the tissue section, as one would expect when the particles at the lower surface are difficult or impossible to visualize. This pattern of z-axis distribution of particles is distinct from the symmetrical ones observed when the stain penetrates the entire tissue section (Fig. 2A–C, Fig. 3A–F; see also Hatton and von Bartheld, 1999), and therefore can not explain the symmetrical profiles, shaped either like a '(or like a')', that were revealed by quantitative z-axis distribution analyses of properly-stained tissue sections. Additional preliminary experiments (data not shown) indicate that the effect of uneven stain penetration can be more subtle than the case shown in Fig. 3F.

We also tested if use of a different fixative, glutaraldehyde, would eliminate z-axis distortion. Previous data showed that z-axis distortion was present regardless of the use of either Methacarn or PFA fixation (Hatton and von Bartheld, 1999). Consistent with these results, analysis of 300 particles in glutaraldehyde-fixed paraffin sections also revealed distortion in the z-axis (6–8% difference between the margins and the core of tissue sections, data not shown). We also tested if z-axis distortion occurs in different brain tissues obtained from other, adult animal species. Preliminary data from adult guinea pig tissue sections through the parabigeminal nucleus fixed with Methacarn and embedded in paraffin showed z-axis distortion (data not shown), albeit to a lesser extent than sections through developing chick oculomotor nuclei. Some of the tissue sections analyzed in this and in a previous study (Hatton and von Bartheld, 1999) were generated in different laboratories (Reno, NV, and Seattle, WA), and we observed no differences in z-axis distortion based on the origin of the tissue sections. We conclude that z-axis distortion is a general phenomenon that is not restricted to specific fixatives, lab equipment, tissues or animal species or ages, although such parameters may influence the extent of z-axis distortion. The possible reasons for varying degrees of z-axis distortion (such as myelin content, particle density or size, developmental age) are currently under investigation.

3.5. Comparison of z-axis distortion in vibratome-, cryo-, paraffin-, celloidin- and methacrylate sections

Since all five major types of tissue sections that are used routinely for cell counting have now been examined for z-axis distortion, it is possible to directly compare properties of these sections and assess implications for optical disector counting. As shown in the synopsis in Fig. 3, the data provide evidence for three different patterns of z-axis distortion. In the first group, comprising paraffin, glycolmethacrylate and vibratome sections, distortion of the z-axis is substantial, and it has the shape of a 'valley in the center' with higher densities at both margins (Fig. 3A–C). Glycolmethacrylate-embedded sections and paraffin sections can show an undulating course of particle distribution along the z-axis, as seen in particular in thicker paraffin or glycolmethacrylate (Hatton and von Bartheld, 1999). Although statistical significance has not been established with these data sets, such 'waves' or alternating zones of decreased and increased densities of particles may suggest that they correlate with alternating zones of decreased and increased compression (Fig. 3C, Fig. 4A). Note that the patterns shown for thinner and thicker cryosections are virtually identical if one takes into account the 'invisible' particles that caused a drop of the average 10% dotted line in cases with uneven stain penetration.

The second pattern is that with an essentially 'flat' curve, indicating minimal distortion. This pattern is seen only in celloidin sections (Fig. 3D). There is still a slight trend for distortion in the same direction as with the first group, but statistical analyses show that there were no significant differences between bins in this case, and the deviations amount to less than 5% and thus appear to be negligible for most practical purposes. In the third group (cryosections), the distortion is minimal, and slightly in the opposite direction, with a bulging in the center (increased density in the center), and a drop-off towards both margins (Fig. 3E). With this kind of pattern, it is not known if the drop-off at the margins could be an artifact, e.g. if the surfaces are rough and there might be lost caps (Andersen and Gundersen, 1999; Section 4). All three patterns are symmetric along the z-axis, meaning that there were no major differences between the densities of particles at the upper surface of tissue sections compared with the bottom of such sections, despite the fact that the upper surface is exposed during tissue processing and staining, while the bottom surface is attached to the glass slide and would be more protected from harsh, particle-dislodging influences during tissue processing. Taken together, our data provide strong evidence for substantial z-axis distortion in 3 of 5 commonly used types of tissue sections. As discussed below, differences in section deformation have important implications for disector counting and also show that different embedding media, protocols, and sectioning devices can have significant and unexpected influences on the distribution of particles in the z-axis of sections.

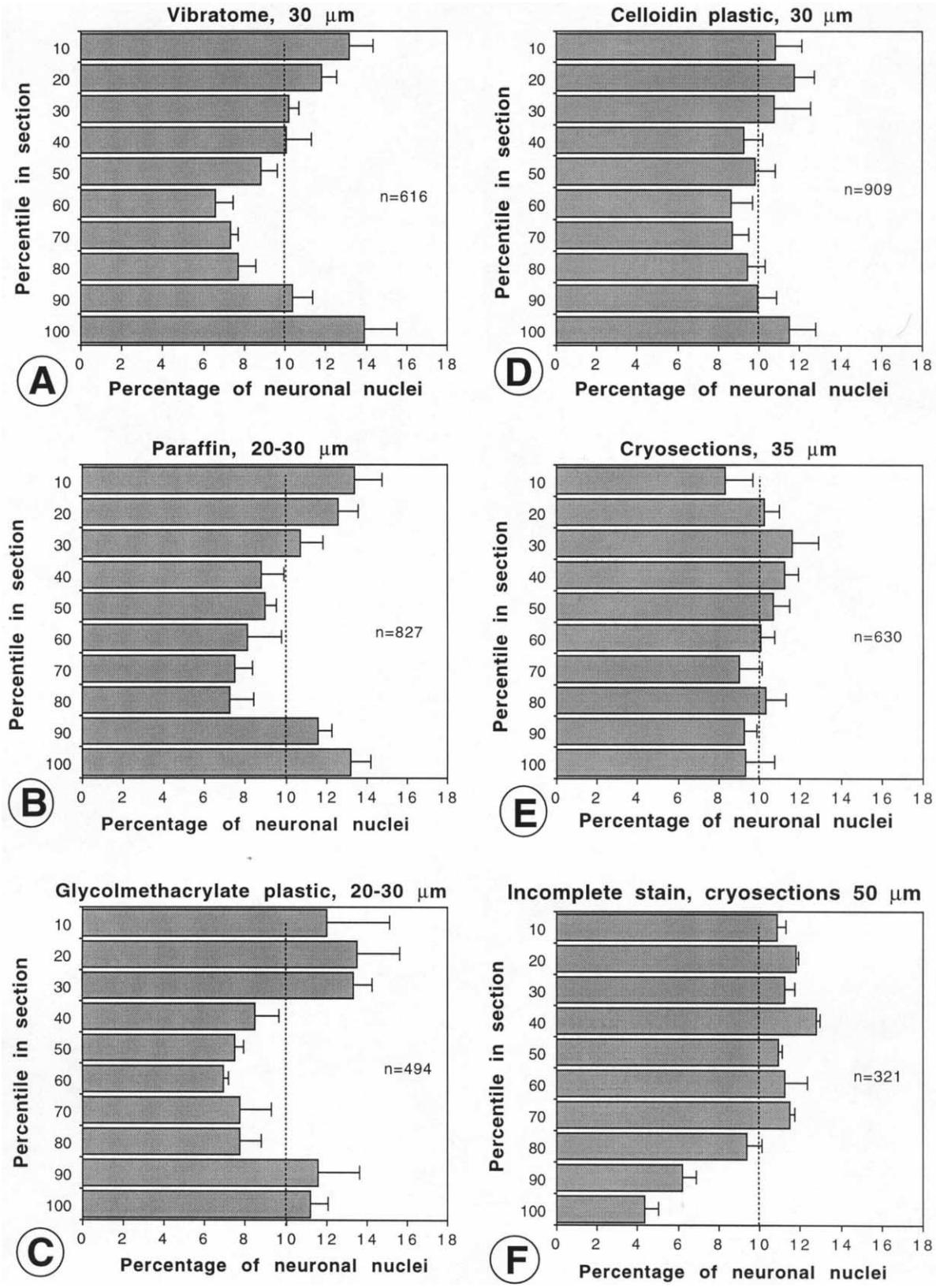

Fig. 3. Synopsis of particle distribution along the z-axis for 5 types of commonly used tissue sections: Vibratome (A), paraffin (B), glycolmethacrylate (C), celloidin (D), cryosections (E). For comparison, an analysis of a section with incomplete stain penetration is included (F). Note that all particle distribution patterns with complete stain penetration (A–E) are symmetrical, while incomplete stain penetration (F) yields an asymmetrical distribution. There are 3 groups that can be distinguished among the five types of tissue sections: low density in the core (A, B, C), basically flat distribution (D), and slightly higher density in the core (E). The vertical dashed line indicates how the particles would present if all visible particles were equally distributed throughout the z-axis. Note that in all sections one can only plot the real and average distribution of visible (stained) particles, but not those that go undetected. Error bars = SEM.

3.6. Mechanism of differential distortion: compression or shrinkage?

There are two main processes that could be responsible for the observed distortion of the z-axis. When the knife blade plows through the tissue block, it causes compression of the tissue, particularly the margins of tissue sections (Williams and Rakic, 1988; Hatton and von Bartheld, 1999; Guillery, 2002). The extent of permanent compression of the margins likely depends on the 'softness' or 'elasticity' of the tissue and embedding medium (Williams and Rakic, 1988; Deverell et al., 1989; Helander, 1983; Ladekarl, 1994; Hatton and von Bartheld, 1999). After the section has been cut, the former edge of the tissue may not 'spring back' into the original extent of the space, thereby causing compression zones of permanently decreased space with a relatively increased particle density (Fig. 1). The other possibility is that during drying (dehydration) of tissue sections, sections may become distorted in the z-axis, because the margins may dry at a different rate than the center (Guillery, 2002). Such distortion might be expected to be asymmetric, with a greater effect on the upper (air) surface than the lower surface (adhered against the glass slide) (Andersen and Gundersen, 1999). We have begun to investigate the cause of the distortion by analyzing the pattern of distortion when the final dehydration step is omitted and the section is coverslipped in water-based mounting media (Aquamount or gel Mount). Although aqueous mounting media have a lower refractive index (1.36) than glass, DPX mountant or tissue (1.51) and thus may behave slightly different than dehydrated and DPX-embedded tissue, this analysis showed a symmetric pattern of particle distribution in the z-axis, with a similar distortion effect in water-based mounting media as in dehydrated, xylene-cleared tissue (Fig. 4A, B). The z-axis distortion shown in Fig. 4A was compared with the distortion shown in Fig. 4B by using Spearman rank order correlation. The patterns were statistically and positively correlated with one another ($r = 0.76$, $P < 0.01$). Thus, the two distortion curves were highly similar, and we conclude that the final dehydration step alone is not responsible for the z-axis distortion.

4. Discussion

There is currently great confusion and debate about the appropriate counting of particles in tissue sections (Coggeshall and Lekan, 1996; Popken and Farel, 1996; Guillery and Herrup, 1997; von Bartheld, 1999; Saper, 1999; West, 1999; Geuna, 2000; Kordower, 2000; Benes and Lange, 2001; von Bartheld, 2001, 2002; Guillery, 2002). While the large majority of investigators continues to use traditional 2D methods (surveyed in: von Bartheld, 2002), it has become clear that 3D methods, such as the optical disector, can have important advantages over 2D methods (West, 1999; von Bartheld, 2002; Guillery, 2002). The 3D method was initially introduced as being 'inherently unbiased' (Gundersen et al., 1988a,b; Cruz-Orive, 1994; Mayhew and Gundersen, 1996; Howard and Reed, 1998), but recent studies have revealed unexpected sources of bias, especially with regard to sampling strategies (Hatton and von Bartheld, 1999). The optical disector has several important

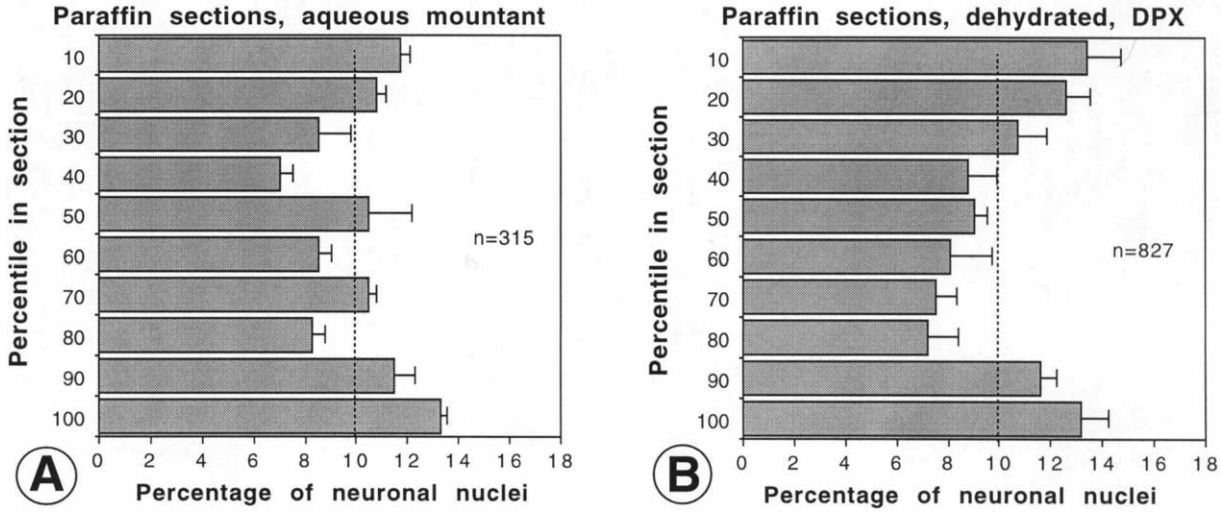

Fig. 4. A, B. Comparison of particle distribution patterns in the z-axis of paraffin sections either coverslipped with aqueous mountants (A) or dehydrated and coverslipped with DPX (B). Note that the general pattern with higher densities in the margins is similar (correlation coefficient = 0.76, Spearman rank order correlation, $P < 0.01$), but that the lower density in the core of the section that was not dehydrated is less pronounced. These data indicate that the basic pattern of z-axis distortion is not caused by the final dehydration step, although final dehydration may have a minor effect on the extent of tissue deformation. The vertical dashed line indicates an equal distribution of particles throughout the z-axis. Error bars = SEM.

qualities: it is relatively easy to use, efficient, and it eliminates some major sources of bias that affect the profile-based counting approaches (Coggeshall and Lekan, 1996; Howard and Reed, 1998; West, 1999). Therefore, it is important to evaluate whether the new potential sources of bias due to z-axis distortion 'disqualify' the optical disector method for such sections, or if such biases can be minimized or eliminated. It is the goal of the current report to help researchers to make rational choices among histological and stereological methods and to improve the accuracy of quantitative data when the optical disector counting method is employed.

4.1. Choices of embedding/sectioning

When designing a quantitative morphological research project, investigators have to choose among histological protocols as well as counting methods. In general, all histological (embedding and sectioning) procedures have advantages and disadvantages, and researchers should carefully consider and be informed about the options (von Bartheld, 2002). Consideration should be given to those embedding and sectioning protocols that will result in the optimal morphology for staining and recognition of the particles of interest. Furthermore, the procedure should be reliable, and easy to follow. Finally, the histological procedures should be compatible with the counting method that will be used for quantification. As has become apparent in recent studies, not all counting methods can be applied indiscriminately to all types of histological sections. Investigators need to carefully weigh advantages and disadvantages and decide which procedures and protocols best serve, overall, the goal of their study. A balance must be found between optimal morphology, easy and simple embedding and sectioning, and efficient, yet minimally biased counting methods. Distortion in the z-axis of tissue sections is one important factor that has to be considered, because different embedding and sectioning protocols are differently affected by z-axis distortion and can potentially result in substantial biases of the optical disector method.

4.2. Is there z-axis distortion in tissue sections?

The present study shows unambiguously that tissue sections can be distorted in the z-axis. This means that tissue sections can have different particle densities along the z-axis (also called 'differential, uniform... deformation of tissue blocks or thick sections in the direction of the z-axis', Dorph-Petersen et al., 2001, p. 234). A reliable technique for assessing such distortion has been developed only recently, and was first systematically and thoroughly applied to different types of tissue sections by Hatton and von Bartheld (1999). This exhaustive study sampled dozens of different conditions of tissue sections to elucidate which parameters affect z-axis distortion, including (1) type of fixative: PFA, Methacarn, (2) type of embedding medium: paraffin, glycolmethacrylate, cryosection, (3) type of sectioning device: glass knife, disposable metal blade, solid metal knife, (4) section thickness: 25–60 μm, (5) stains: thionin, neutral red, toluidine blue. These studies indicated that the embedding medium was the most important factor in determining the direction (increased or decreased particle densities) and degree of z-axis distortion. The present account complements this analysis by adding vibratome and celloidin sections, and by showing that the bimodal distributions cannot be explained by incomplete stain penetration, since this would lead to asymmetric patterns, while all observed z-axis distortion patterns were symmetric (Figs. 3 and 6). Taken together, the data confirm that different embedding media facilitate different patterns and degrees of distortion of particle density in the z-axis of sectioned tissues. In addition, the evidence now overwhelmingly shows that distortion of particle density in the z-axis is a real phenomenon that has to be addressed, and cannot be explained away as a 'staining artifact' (Dorph-Petersen et al., 2001). However, this does not mean that all vibratome, paraffin or glycolmethacrylate sections are distorted in the z-axis, but merely that the potential exists that they might be. Only when many different types of sections and procedures have been tested for z-axis distortion (and those results are reported in publications), will it be possible to assess the extent to which such sections are affected by z-axis distortion and which procedures and parameters of the tissue may be responsible for the distortion.

4.3. Apparent discrepancies with a previous vibratome section analysis

Andersen and Gundersen (1999) used a basically similar, but more limited approach (one analysis of 187 particles) than our particle density distribution analysis, to assess the loss of cell nuclei from vibratome sections. They concluded (1) that particle distribution within 70% comprising the core of the z-axis was 'fairly uniform', (2) that the nearly 100% increased particle density at the near-bottom zone of the section was 'not clearly different from the expected', and (3) that the almost complete depletion of neuronal nuclei within the uppermost and to a lesser extent the lowest zones of the z-axis was due to lesioning of the neuronal nuclei by the knife and subsequent removal of those nuclei during tissue processing, making the use of guard spaces mandatory.

We agree that conclusion (1) may be correct, but, most importantly, this does not ensure that the observed particle density in the core is representative for the

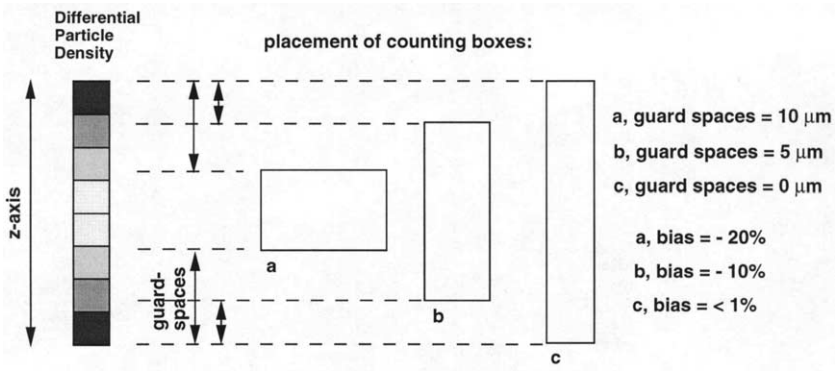

Fig. 5. Illustration of the strategy that uses placement and extent of counting boxes for sampling as a tool to minimize the biases caused by differential particle density in tissue sections. The cartoon illustrates three different shapes of counting boxes (a, b, c) that can be placed along the z-axis as indicated. When particles are distributed with differential densities as indicated on the left, the placement of counting boxes will reflect the true, representative particle density to different degrees. The size of the guard spaces varies accordingly.

section as a whole. Furthermore, based on our one-way ANOVA with vibratome sections, a larger number of particles (at least 250 particles) needs to be analyzed for definitive conclusions. Regarding conclusion (2), we argue that the observed spike was likely significant, and a larger number of sampled particles than 187 would have shown this, as this pattern is very similar to the one that we consistently observe in our vibratome sections (Fig. 2A). Regarding conclusion (3), it is obvious that the particle distribution within the vibratome sections analyzed by Andersen and Gundersen (1999) was very different than the one that we observed here. Obviously, even seemingly minor differences in the details of tissue processing can lead to significant differences in the extent of damage of particles or z-axis distortion. This further underscores the necessity to analyze the patterns of particle distribution within the z-axis for many sets of sections (Guillery, 2002).

There could be multiple reasons for the poor retention of neuronal nuclei in the margins of sections in the study by Andersen and Gundersen (1999). First, their tissue was not perfusion-fixed, but was human material, fixed presumably some time (no information given) after the death of the individual. In our study, the animals were perfused intracardially with 4% PFA, likely resulting in superior fixation. Second, the human sections were baked at 60 °C to the slide rather than air-dried at room temperature. Third, the human sections were stained with Giemsa for 3.5 h, rather than stained with thionin for 5 min. Giemsa stain requires acetone and acid pH for proper staining (Vacca, 1985), especially when using formaline-fixed tissue. Such differences of tissue preparation and processing likely had effects on the integrity and retention of neuronal nuclei in the margins of the tissue sections. Accordingly, it is important to verify the pattern of distortion prior to sampling for optical disector estimates. In our view, sections with such dismal retention of particles in the margins (up to one third of the entire section was severely depleted) as reported by Andersen and Gundersen (1999) have to be used with great caution for quantitative studies, because with such a profound loss of particles, it is impossible to know whether the margins originally contained an increased, a decreased,

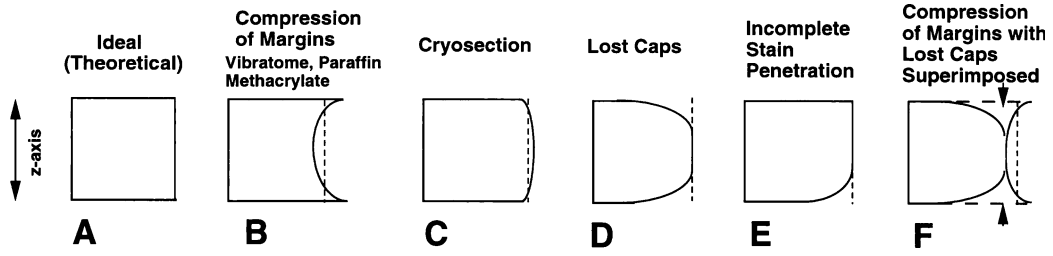

Fig. 6. (A–F) Highly schematic drawings showing some perceived and some real distortions of particle densities in the z-axis of tissue sections. We emphasize that these cartoons are highly schematic and merely illustrate the basic possibilities, but do not necessarily reflect the distortions proportionally or to scale. The 'true' (= truly representative) density of particles that should be used for estimates of particle numbers is indicated by the vertical dashed line (B–F). (A) Ideal situation with completely equal densities in the margins and the core. (B) Compression of margins results in higher particle densities at the margins, as seen in vibratome, paraffin and methacrylate sections. (C) Slightly lower densities in the margins as seen in cryosections. (D) Extreme loss of particles ('lost caps') in the margins as described for poorly-preserved vibratome sections (Andersen and Gundersen, 1999). (E) Apparent 'loss' of particles from the margin dried against the glass slide in the case of incomplete stain penetration. (F) Margins are compressed, resulting in increased densities of particles at the margins, but particles are secondarily lost from the margins due to poor tissue preservation, resulting ultimately in a lower density of particles (arrows) than was actually present in the tissue block (vertical dashed line).

or an average density of particles (Fig. 6F). Unfortunately, this pattern of particle loss at margins appears to be common among human, generally poorly fixed tissues (K.-A. Dorph-Petersen, personal communication), meaning that in such tissues about 30% of the particles are systematically excluded from proper evaluation. This underscores the importance of checking the quality of tissue sections ('quality control') prior to embarking on any quantitative approach, but especially when using the optical disector that relies on sampling and thus on the fundamental principle that each particle must have the same chance of being counted.

Distortion of particle distribution in the z-axis can be attributable to lost caps or to differential compression or shrinkage. If only lost caps are involved, then this can be fixed by using guard spaces. If only compression/shrinkage is involved, then this can be fixed by the opposite strategy—minimizing guard spaces. If there is a severe loss of particles or a combination of lost caps and compression/shrinkage, then it is impossible to obtain accurate counts. It is curious, but important, that seemingly similar problems require very different solutions, based on the properties of the tissue sections.

4.4. Practical implications for OD counting

The optical disector was introduced with the notion that the best sampling zone within the z-axis was within the center of sections, because then edge artifacts caused by uneven surfaces and 'lost caps' (Hedreen, 1998a) can be avoided, and the space below or above the counting box can be utilized to unambiguously identify and determine whether the particle fulfills the inclusion criteria for counting (Gundersen et al., 1988a; Williams and Rakic, 1988; Howard and Reed, 1998). This approach is theoretically valid, but assumes that there are no influences of the sectioning procedure or subsequent steps in the treatment of sections that might affect the distribution of particles in the z-axis (Figs. 5 and 6A–F). As mentioned above, it is a fundamental principle of counting techniques that employ sampling that each particle must have the same chance of being counted (Gundersen et al., 1988a; Coggeshall and Lekan, 1996; Howard and Reed, 1998). This principle must also apply to the tissue section after it has been sectioned and processed. Thus, it has to be shown that the particle distribution along the z-axis has not been distorted (that there is no differential distribution) due to influences such as cutting or dehydration. Previous analyses of three types of tissue sections (paraffin, glycolmethacrylate plastic, and cryosections) have shown that two of these three section types, paraffin and glycolmethacrylate plastic, can be substantially distorted in the z-axis, resulting in large biases (up to 25%, Hatton and von Bartheld, 1999), when guard spaces are used as recommended (Gundersen et al., 1988b; Williams and Rakic, 1988; Howard and Reed, 1998). The present study completes this analysis for two other major types of sections, vibratome and celloidin plastic. We show that one type, vibratome sections, is also distorted, while celloidin sections are only minimally affected. So does this mean that the optical disector should not be used for paraffin-, methacrylate or vibratome sections, but only for cryosections and celloidin sections? We do not endorse this view. Both cryosections and celloidin sections also have some major disadvantages: Cryosections render mediocre morphology and are not ideal for recognition of fine features of particles. Celloidin sections provide excellent morphology, but unfortunately the embedding procedure is laborious in terms of time and effort, staining of sections can be tricky, and the materials are expensive (Rosen and Williams, in press). Therefore, the simple and reliable paraffin embedding and sectioning method that furthermore renders excellent morphology should not be regarded as obsolete.

4.5. Strategies for coping with z-axis distortion

Since z-axis distortion is substantial in three types of tissue sections examined (paraffin, glycolmethacrylate, and vibratome sections), optical disector counting has to deal with the bias that results from the use of guard spaces in this counting method. Basically there are four different strategies to cope with z-axis distortion.

(1) The first is to abandon those embedding or sectioning protocols that lead to z-axis distortion, or not to use the optical disector at all on such sections (Dorph-Petersen et al., 2001).

(2) The second is to eliminate or to minimize guard spaces in those sections (Fig. 5). This can be done when the particles of interest are easily recognized, relatively large, of a homogenous shape (Hatton and von Bartheld, 1999), but not when there is evidence for significant loss of particles (lost caps) from the margins of sections (Andersen and Gundersen, 1999). If there is indication of such depletion, and if there is in addition evidence for z-axis distortion, no counting technique can be used with confidence, because it is very difficult if not impossible to 'reconstruct' how many particles have been lost, and which particle densities should be used for those affected zones. Obviously, any bias will be smaller when the sections are thicker and the guard zones are relatively thin.

(3) The third strategy is to determine the pattern of z-axis distortion by measuring the position of at least 250–350 particles as described in Section 2.3, and then to place the counting boxes for sampling in zones such that undershoot and overshoot balances out, resulting in a sampled density that is representative for the entire z-axis (Fig. 5). This can be done with simple equipment (needed anyway for applying the optical disector) and

just a few hours of extra time, and based on information which bins within the z-axis are truly representative for the whole section, the counting boxes can be placed in these zones within the z-axis. This strategy is advised in cases with 'undulating' zones of alternating lower and higher densities as shown in Fig. 4A, and/or when particles are difficult to identify and guard spaces are deemed essential for particle recognition.

(4) The fourth option is to determine the pattern of z-axis distortion as described in Section 2.3, and then to sample only in a defined zone within the center of the section, but to apply a correction factor for the sampled densities. Application of a correction factor (directly obtained through the z-axis distribution analysis) will convert the under- (or over-sampled) zones into data that are representative for the particle density of the entire z-axis of the tissue sections. Since the predicted bias can be calculated easily, one knows the percentage undercount (or overcount) due to the z-axis distortion, and thus can correct sample densities that are not representative for the entire z-axis (Fig. 5). For example, if one wishes to sample in the center 15 μm of a 25 μm section, and one knows that the corresponding bins (30–80 percentiles in Fig. 3A–C) have a 10% undercount (9% instead of 10% of all particles present in those bins), then one can sample and obtain density counts of particles in the 15 μm center, but one needs to apply a 10% increase (+10% correction factor) to make the density of particles representative for the entire section. The resulting estimate should be unbiased with respect to the z-axis distortion.

The choice of either of these strategies will depend on how easy it is to recognize the particles of interest, and whether or not the investigator believes that he or she can afford to eliminate or minimize guard spaces. It is probably not necessary to repeat the z-axis measurements (described in Section 2.3) for each and every study. We recommend to do this analysis when a protocol is used for the first time, not only to detect z-axis distortion, but also to verify complete stain penetration throughout the z-axis (easily detected by a symmetric particle distribution profile). If the same protocol is used for other studies, and none of the crucial parameters have changed (e.g. tissue type, tissue processing, embedding medium, section thickness, or sectioning device), it is reasonable to assume that the initial analysis is still valid. It may be prudent to occasionally 'calibrate' the system to make sure that no crucial parameters have changed.

4.6. Causes of z-axis distortion

It is still unclear which factors are responsible for the differential z-axis distortion seen in tissue sections. Two main factors may play a role: direct compression of the margins of tissue sections when the knife blade plows through the block of tissue (Williams and Rakic, 1988; Hatton and von Bartheld, 1999), and deformations caused by drying and dehydration of tissue sections collected on glass slides (Guillery, 2002). Despite the fact that cryosections shrink considerably due to dehydration (Coggeshall and Lekan, 1996), they are minimally affected by z-axis distortion (and the distortion actually goes in a different direction than in all other types of sections). This supports the notion that compression rather than shrinkage is the major factor responsible for distortion. Our data on tissue sections coverslipped with aqueous mountants also favor compression rather than dehydration as the major cause for z-axis distortion. However, the fact that the center of the aqueous-mounted sections showed somewhat higher densities than the dehydrated sections may indicate that dehydration also has some effects on particle distribution in the z-axis.

Acknowledgements

This work was supported by NIH grants MH 62009 (G.D.R.), HD 043347 and EY 12841 (C.S.v.B.), and NCRR P20 15581 (C.S.v.B., W.J.H.) (Center of Biomedial Research Excellence). We thank Rob Williams for encouragement, and Karl-Anton Dorph-Petersen for insightful discussions. We also thank Lorraine Gibbs, University of Washington, Seattle, and Gary Rondeau (Applied Scientific Instrumentation, Inc., Eugene, OR) for technical advice, and Nick Spencer, University of Nevada, Reno, for providing guinea pig brain tissue.

References

Abercrombie M. Estimation of nuclear populations from microtome sections. Anat Rec 1946;94:239–47.

Andersen BB, Gundersen HJ. Pronounced loss of cell nuclei and anisotropic deformation of thick sections. J Microsc 1999;196:69–73.

Avendano C, Dykes RW. Quantitative analysis of anatomical changes in the cuneate nucleus following forelimb denervation: a stereological morphometric study in adult cats. J Comp Neurol 1996;370:491–500.

Benes FM, Lange N. Two-dimensional versus three-dimensional cell counting: a practical perspective. Trends Neurosci 2001;24:11–7.

Clarke PGH. An unbiased correction factor for cell counts in histological sections. J Neurosci Methods 1993;49:133–40.

Clarke PGH, Oppenheim RW. Neuron death in vertebrate development: in vitro methods. Methods Cell Biol 1995;46:277–321.

Coggeshall RE, Chung K. The determination of an empirical correction factor to deal with the problem of nucleolar splitting in neuronal counts. J Neurosci Methods 1984;10:149–55.

Coggeshall RE, Lekan HA. Methods for determining numbers of cells and synapses: a case for more uniform standards of review. J Comp Neurol 1996;364:6–15.

Cruz-Orive LM. Towards a more objective biology. Neurobiol Aging 1994;15:377–8.

Deverell MH, Bailey N, Whimster WF. Tissue distortion in three-dimensional reconstruction of wax or plastic embedded microscopic structures. Pathol Res Pract 1989;185:598–601.

Dorph-Petersen KA, Nyengaard JR, Gundersen HJ. Tissue shrinkage and unbiased stereological estimation of particle number and size. J Microsc 2001;204:232–46.

Gardella D, Hatton WJ, Rosen GD, von Bartheld CS. Differential distortion of the z-axis in tissue sections: implications for optical disector counting. Soc Neurosci Abstr 2002;28 (#505.15).

Geuna S. Appreciating the difference between design-based and model-based sampling strategies in quantitative morphology of the nervous system. J Comp Neurol 2000;427:333–9.

Guillery RW. On counting and counting errors. J Comp Neurol 2002;447:1–7.

Guillery RW, Herrup K. Quantification without pontification: choosing a method for counting objects in sectioned tissues. J Comp Neurol 1997;386:2–7.

Gundersen HJG, Bagger P, Bendtsen TF, Evans SM, Korbo L, Marcussen N, et al. The new stereological tools: disector, fractionator, nucleator and point sampled intercepts and their use in pathological research and diagnosis. Acta Pathol Microbiol Immunol Scand 1988a;96:857–81.

Gundersen HJG, Bendtsen TF, Korbo L, Marcussen N, Møller A, Nielsen K, et al. Some new, simple and efficient stereological methods and their use in pathological research and diagnosis. Acta Pathol Microbiol Immunol Scand 1988b;96:379–94.

Hatton WJ, von Bartheld CS. Analysis of cell death in the trochlear nucleus of chick embryos: Calibration of the optical disector counting technique reveals systematic bias. J Comp Neurol 1999;409:169–86.

Hedreen JC. Lost caps in histological counting methods. Anat Rec 1998a;250:366–72.

Hedreen JC. What was wrong with the Abercrombie and empirical cell counting methods. A Rev Anat Rec 1998b;250:373–80.

Heinsen H, Arzberger T, Schmitz C. Celloidin mounting (embedding without infiltration)—a new, simple and reliable method for producing serial sections of high thickness through complete human brains and its application to stereological and immunohistochemical investigations. J Chem Neuroanat 2000;20:49–59.

Helander KG. Thickness variations within individual paraffin and glycol methacrylate sections. J Microsc 1983;132:223–7.

Herman AE, Galaburda AM, Fitch RH, Carter AR, Rosen GD. Cerebral microgyria, thalamic cell size and auditory temporal processing in male and female rats. Cereb Cortex 1997;7:453–64.

Howard CV, Reed MG. Unbiased stereology. Three-dimensional measurement in microscopy. New York: Springer, 1998:246.

Konigsmark BW. Methods for the counting of neurons. In: Nauta WJH, Ebbesson SOE, editors. Contemporary research methods in neuroanatomy. New York: Springer, 1970:315–40.

Kordower JH. Making the counts count: the stereology revolution. J Chem Neuroanat 2000;20:1–2.

Ladekarl M. The influence of tissue processing on quantitative histopathology in breast cancer. J Microsc 1994;174:93–100.

Mayhew TM, Gundersen HJ. If you assume, you can make an ass out of u and me': a decade of the disector for stereological counting of particles in 3D space. J Anat 1996;188:1–15.

Nurcombe V, Wreford NG, Bertram JF. The use of the optical disector to estimate the total number of neurons in the developing chick lateral motor column: effects of purified growth factors. Anat Rec 1991;231:416–24.

Popken GJ, Farel PB. Reliability and validity of the physical disector method for estimating neuron number. J Neurobiol 1996;31:166–74.

Rosen GD, Williams RW. Complex trait analysis of the mouse striatum: independent QTLs modulate volume and neuron number. BMC Neurosci 2001;2:5.

Rosen GD, Williams RW. Celloidin embedding and cresyl violet staining. Current Protocols in Neuroscience, in press.

Saper CB. Unbiased stereology: three-dimensional measurement in microscopy. Book review. Trends Neurosci 1999;22:94–5.

Schmitz C, Korr H, Perl DP, Hof PR. Advanced use of 3-D methods for counting neurons. Trends Neurosci 2001;24:377–80.

Selemon LD, Rajkowska G, Goldman-Rakic PS. Elevated neuronal density in prefrontal area 46 in brains from schizophrenic patients: application of a three-dimensional, stereologic counting method. J Comp Neurol 1998;392:402–12.

Stuart DA, Oorschot DE. Embedding, sectioning, immunocytochemical and stereological methods that optimise research on the lesioned adult rat spinal cord. J Neurosci Methods 1995;61:5–14.

Uylings HB, van Eden CG, Hofman MA. Morphometry of size/volume variables and comparison of their bivariate relations in the nervous system under different conditions. J Neurosci Methods 1986;18:19–37.

Vacca LL. Laboratory manual of histochemistry. New York: Raven, 1985:578.

von Bartheld CS. Counting particles in tissue sections: choices of methods and importance of calibration to minimize biases. Histol Histopathol 2002;17:639–48.

von Bartheld CS. Systematic bias in an 'unbiased' neuronal counting technique. Anat Rec (New Anat) 1999;257:119–20.

von Bartheld CS. Comparison of 2D- and 3D-counting: the need for calibration and common sense. Trends Neurosci 2001;24:504–6.

West MJ. Stereological methods for estimating the total number of neurons and synapses: issues of precision and bias. Trends Neurosci 1999;22:51–61.

Williams RW, Rakic P. Three-dimensional counting: accurate and direct method to estimate numbers of cells in sectioned material. J Comp Neurol 1988;278:344–52.